

# Simulation of exoplanetary clouds in transit light curves

Werner Elst

April 25, 2022

*Context.* Clouds are frequently present in exoplanetary atmospheres. For further investigation more data has to be collected. Predicting which conditions a cloudy exoplanet must satisfy to be discernible from his cloudless counterpart is essential to not misuse any telescope time.

*Aims.* We present a straightforward model to predict the influence of non-uniform cloud coverage on the transit light curve. We also provide an idea of how feasible it is to observe cloud coverage with different ground- and space-based telescopes.

*Method.* We added conditions to customary models of cloudless exoplanet transits. The model thus obtained was used to generate synthetic light curves for a multitude of cloudy planets satisfying realistic bulk and orbital parameters. These light curves were then compared to their cloudless counterparts.

*Results.* We find that depending on the telescope used and depending on the bulk and orbital parameters of the exoplanet observed, inhomogeneous cloud coverage should be observable.

## 1. Introduction

Since the first discovery of an exoplanet in 1992 by Wolszczan & Frail (1992) the amount of confirmed detections has boomed, mainly thanks to transit photometry <sup>1</sup>. To better understand these light curves many models have been created, most famously in an analytical way by both (Mandel & Agol 2002) and by Giménez (2006).

A decade after the first exoplanet discovery Charbonneau et al. (2002) were the first to report the detection of an exoplanetary atmosphere. Upon further investigation of exoplanets and their atmospheres using transit spectroscopy in the near-IR and the optical (data gathered by i.a. Hubble Space Telescope), astronomers noticed the lack of certain anticipated atomic/molecular features. It has been theorized that this lack is a result of cloud coverage.

Clouds may affect the planet's atmosphere by depleting elements and via scattering and absorption. In this way clouds can have a major effect on the balance between incoming energy (originating from the host star) and outgoing energy. Much has still to be learned about exoplanetary clouds and their effects on the atmosphere. Observing exoplanets with cloud coverage is an essential part of

---

<sup>1</sup>[exoplanets.nasa.gov](http://exoplanets.nasa.gov)

this learning process, being able to predict the constraints to be fulfilled by an exoplanet to be able to detect cloud coverage prevents us from wasting expensive telescope time.

A nice overview of the current state of affairs vis à vis exoplanetary clouds is given by (Helling 2019).

## 2. Methods

First we will give a description of the model: setup, parameters used, etc., then we give an explanation of the computational procedure and lastly, we describe how the flux at each point in time is calculated.

### 2.1. Model description

Our model is inspired by the model described by von Paris et al. (2016) (in section 3) and a general setup can be seen in Figure 1.

We start out by defining a  $N \times N$  grid, which for our simulations was taken to be  $2000 \times 2000$  for computational time sake. This grid we use to compute the luminosity of the star and to keep track of which part of the star is covered by the planet/cloud (more precise description later in this section). The center of the star is chosen to coincide with the center of the grid and defines the center of an  $(x,z)$ -coordinate system.

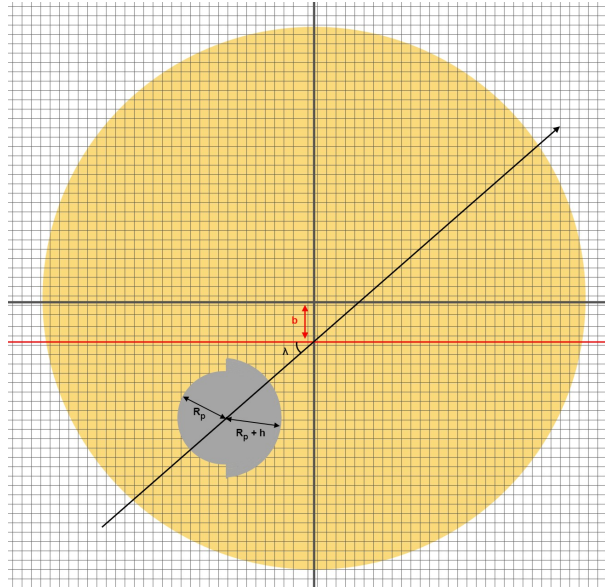


Figure 1: Depiction of our model setup. Not to scale. The leading part of the planet is covered by clouds with height  $h$ . The planet moves in the direction indicated by the arrow, it misses the star's center by impact parameter  $b$  and has a spin-orbit angle  $\lambda$ .

The planet with cloud coverage is described as two half circles, one half with radius  $R_p$  and the other with radius  $R_p + h$ , where  $R_p$  is the planet's radius and  $h$  is the height of the cloud. We allow for  $h$  to be both positive and negative which we interpret as a leading, trailing cloud coverage respectively.

For simplicity we assume the star and the planet to be spherical, this is not entirely correct but for slowly rotating stars distortions due to rotation of only  $\frac{\Delta R}{R} = (1.8 \pm 0.6) \times 10^{-6}$  have been reported (Gizon et al. 2016). Fast rotating stars may show large distortions and therefore the model in its current state is not able to describe transits in such situations entirely correctly, this is mentioned in section 5 on future prospects.

For the description of the stellar surface, a general limb-darkening law is adopted, as given by:

$$I_*(\mu) = I(0) \times \left( 1 - \sum_{n=1}^N u_n (1 - \mu^n) \right) \quad (1)$$

where  $I(0)$  is the star's central intensity,  $u_n$  are the limb-darkening coefficients,  $\mu = \cos(\gamma)$  and  $\gamma$  is the angle of foreshortening (the angle between the local normal to the surface and the line of sight). In our coordinate system we can rewrite  $\mu$  as follows:

$$\begin{aligned} \cos^2(\gamma) \cdot R_*^2 &= R_*^2 - (x^2 + z^2) \\ &\downarrow \\ \mu \equiv \cos(\gamma) &= \sqrt{1 - \frac{x^2 + z^2}{R_*^2}} \end{aligned} \quad (2)$$

Depending on the situation we want to simulate the limb-darkening law can be taken to be linear, quadratic or of even higher order. In transit modeling a quadratic order limb-darkening is generally accepted.

We have five orbital parameters: semi-major axis  $a$ , eccentricity  $e$ , inclination  $i$ , spin-orbit angle  $\lambda$  and period  $P$ .

The semi-major axis we leave as a completely free parameter that can be tuned to whatever situation we want to have a look at.

The eccentricity is always taken zero. This was done as not to make the model too complex but  $e \neq 0$  would certainly be a nice extension in the future. Keeping the eccentricity fixed to zero is overall not a bad assumption as shown by Esteves et al. (2015).

The inclination is the angle between the plane of the sky and the planet's center measured when the planet's center passes the  $z$ -axis. Using this orbital inclination we can define the impact parameter  $b$  in the following way:

$$b \cdot R_* = \sin(i) \cdot a \quad (3)$$

shown in red in Figure 1. The inclination equals zero when the planet's center is exactly on the positive  $z$ -axis and  $\frac{\pi}{2}$  when  $z = 0$ .

The spin-orbit angle  $\lambda$ , also shown in Figure 1, is the angle between the star's plane of rotation (assumed to be perpendicular to the plane of the sky) and the planet's plane of orbit.

When the spin-orbit angle is a multitude of  $\frac{\pi}{2}$  the inclination is taken as the angle between the plane of the sky and the planet's center measured when the planet's center passes the  $x$ -axis.

Notwithstanding the fact that we have the semi-major axis as a parameter, we add the period as a

Telescope	Noise (ppm)
NGTS <sup>a</sup>	500
TESS <sup>b</sup>	10 <sup>3</sup>
Kepler <sup>c</sup>	29
CHEOPS <sup>d</sup>	20

<sup>a</sup> taken from Wheatley et al. (2017).

<sup>b</sup> taken from Campante et al. (2016).

<sup>c</sup> taken from Gilliland et al. (2011).

<sup>d</sup> taken from Benz et al. (2021).

Table 1: Overview of the noise levels assumed for 1 ground-based (namely NGTS) and 3 space-based telescopes.

parameter and thereby constrain the stellar mass via Kepler’s third law instead of vice versa (as is often done). This was not done with any particular reason in mind.

We can deduce from the period in combination with the planet’s trajectory the actual time the planet spends in front of the star, this can eventually be seen in the light curve.

The amount of time steps can be fine tuned to anyone’s liking and is in this paper taken to be always 100 from the start of the transit until the end of the transit. To better visualize the baseline 25 points have been added before and after the transit.

The time steps can also be tuned as to sample more points during ingress and egress and less during the portion of time the planet is entirely in front of the star. In our standard setup we take 2/5<sup>th</sup> of the steps in time (so 40 points) are taken during ingress, 1/5<sup>th</sup> during full transit and 2/5<sup>th</sup> during egress. This feature was added because the interesting parts for us are the ingress and the egress.

Lastly, synthetic Gaussian noise is added to the simulated light curve. The  $\sigma$  can be freely chosen, in this paper we mimic the errors of four telescopes, listed in Table 1, one ground-based telescope and three space-based telescopes.

## 2.2. Computational procedure

After defining all of the above mentioned parameters the actual computational part starts.

First we begin by figuring out where the planet intersects the star for the first time and the last time. This is simply done by formulating a system of equations describing the path of the planet’s center and the circumference of a circle with radius equal to that of the star plus that of the planet plus the (absolute value of the) cloud height:

$$\begin{cases} \tan(\lambda) \cdot x + b & = z \\ (R_* + R_p + |h|)^2 & = x^2 + z^2 \end{cases} \quad (4)$$

If this system has two solutions the planet will cross the star, if it has only one solution the planet will touch the star and if there are no solutions the planet completely misses the star.

This approach has two major advantages:

- If the planet only touches or completely misses the star, we can raise an exception and the code immediately stops running, without wasting any time.
- If we used basic trigonometry with our starting parameters, we might have found a starting point very far away from the star and unless a cumbersome procedure to skip the uninteresting part was introduced, we would waste a lot of computational time calculating the flux when the planet is still outside of the star. By determining the exact starting and ending point of the transit in our way we circumvent this problem.

Unfortunately, there is one big disadvantage. When  $\lambda$  approaches a multitude of  $\frac{\pi}{2}$ , the  $\tan(\lambda)$  blows up and strange code behavior may be expected. In the current state of the code an extra condition is defined that if  $\lambda$  is a multitude of  $\frac{\pi}{2}$ , the starting and ending point are found via basic trigonometry. We think we found a better solution but because of a lack of time we weren't able to implement and thoroughly test this solution. A description of the solution is given in section 5 on future prospects.

Hereafter, we do repeat the same procedure only replacing the circle's radius by the star's radius. If there are 0 or 1 solution(s) the planet only grazes the star, if there are 2 solutions we have to check whether the planet is fully inside the star when the planet's center is at its point of closest approach to the star's center. The distance of closest approach is given by:

$$l = \begin{cases} \frac{|b|}{\tan(\lambda)} \cdot \sin(\lambda) & \text{if } 0 \leq \lambda - n\pi \leq \frac{\pi}{2} \\ \frac{|b|}{\tan(\pi-\lambda)} \cdot \sin(\pi - \lambda) & \text{if } \frac{\pi}{2} \leq \lambda - n\pi \leq \pi \end{cases} \quad (5)$$

where  $n \in \mathbb{Z}$ .

If the planet is completely inside the star at closest approach we have a full transit, else the planet only grazes the star.

When the star grazes we have to adjust the oversampling of the ingress and egress to get an equally sampled light curve.

After this, we really start setting up a grid and going over all the grid points, adding up their intensities as defined in the next subsection, for each point in time. Then the same is done for a planet without any clouds with the same total area, as for example analytically described by (Mandel & Agol 2002) or (Giménez 2006). The resulting curves are plotted in one graph and the  $1\sigma$ -interval is added around the asymmetric curve.

Lastly, the difference between the symmetric and asymmetric curves are plotted in a residual plot in the hope of finding a pattern that indicates the asymmetry due to the cloud.

### 2.3. Flux determination

In the remaining part of this section we describe how the flux at a certain point in time is calculated in our model.

At each of our points in time we want to determine the normalized flux:

$$F = \frac{\iint I(x, z) dx dz}{\iint I_*(x, z) dx dz} \quad (6)$$

where the numerator represents the flux at a certain point in time during transit and the denominator represents the flux when nothing blocks the stellar light.

The intensity  $I_*(x, z)$  in the denominator is given by the aforementioned limb-darkening law (1).

The intensity  $I(x, z)$  in the numerator is given by the following conditions:

$$I(x, z) = \begin{cases} 0 & \text{if } x^2 + z^2 \geq R_*^2, \\ 0 & \text{if } (x - x_p)^2 + (z - z_p)^2 \leq R_p^2, \\ 0 & \text{if in cloud,} \\ I_*(\mu) & \text{otherwise.} \end{cases} \quad (7)$$

where  $x_p$  and  $z_p$  are the coordinates of the planet's center. The first line represents a point outside the star (we assume there are no background stars). The second line are points inside the planet, the third line points inside the cloud and the fourth line are points on the star's surface.

The conditions for a point to be situated inside the cloud are:

$$\text{True if } \begin{cases} x^2 + z^2 \leq R_*^2, \\ (x - x_p)^2 + (z - z_p)^2 > R_p^2, \\ (x - x_p)^2 + (z - z_p)^2 \leq (R_p + h)^2, \\ h \cdot (x - x_p) \geq 0. \end{cases} \quad (8)$$

The first line states that points lie inside the star. The second line expresses that the point must not lie inside the planet. The third line makes sure that the point lies within the cloud height and the fourth line assures that the point lies in the leading/trailing part depending on  $h$  being either positive or negative.

### 3. Results

In the first simulation we model a Jupiter-like planet around a sun-like star but with  $i = 0$ ,  $\lambda = 0$  and  $a = 1$  AU. All the parameters used are summarized in Table 2.

The light curve obtained from this simulation is shown in Figure 2. The black dots are the data points of the planet with cloud coverage and Gaussian noise as expected from NGTS, the red line is the light curve of the cloudless planet, the blue (not visible) line is the mean of the cloudy planet's light curve and the light blue region represents the  $1\sigma$ -interval of the NGTS noise. The curvy line during full transit (between the dotted lines) is due to limb-darkening. It can be immediately seen that with NGTS discerning the cloud will not be possible.

The effect of the cloud coverage on the residuals is shown in Figure 3. If there was no noise (red line) a distinct pattern would be discernible, and in its extremes an effect of up to 100 ppm would show. Because of the noise, which is large as compared to the cloud coverage effect, no pattern can be recognized in the black dots.

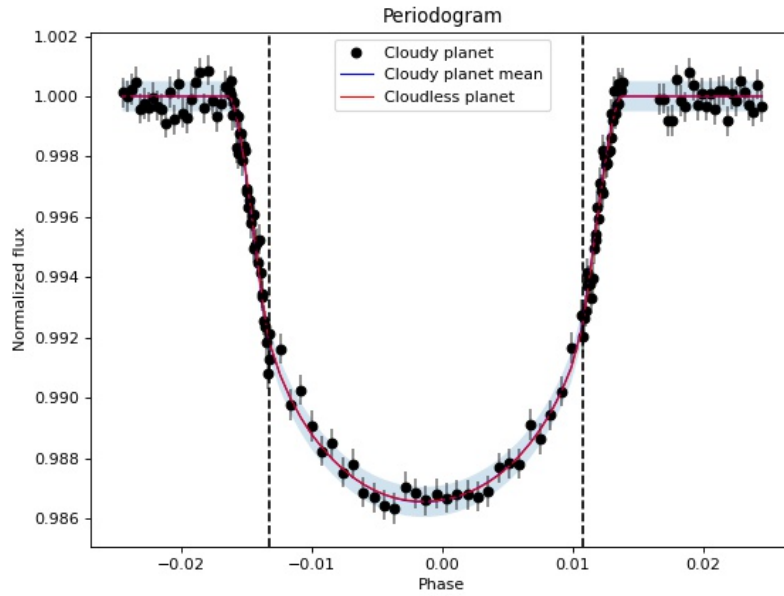


Figure 2: The light curve obtained for a Jupiter-like planet with  $h_{\text{cloud}} = 2, 100$  km passing in front of a sun-like star. The cloudy planet's mean light curve coincides so much with its cloudless counterpart that is not visible in this figure. The noise resembles the NGTS', the light blue region represents the  $1\sigma$ -interval around the cloudy planet's mean light curve. The black dotted lines show the region where the planet is completely in front of the host star.

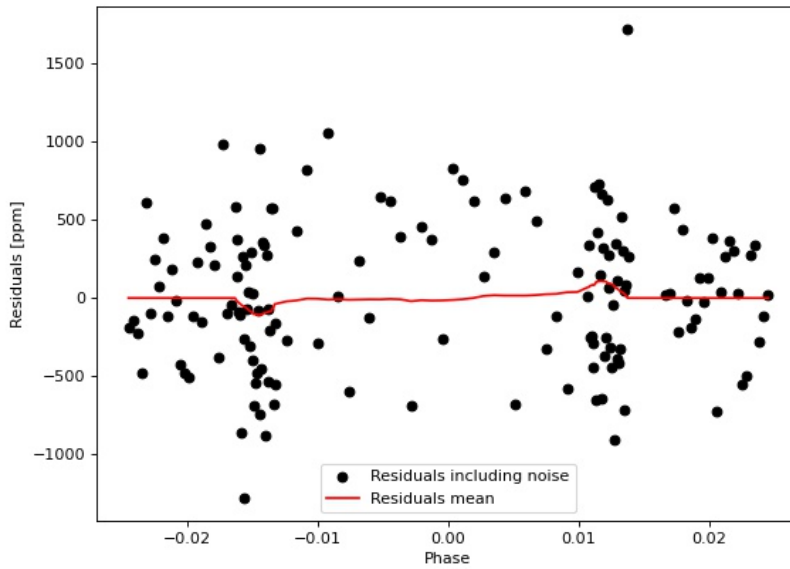


Figure 3: The residuals between a symmetric and an asymmetric model obtained for a Jupiter-like planet with  $h_{\text{cloud}} = 2, 100$  km passing in front of a sun-like star. The noise resembles the NGTS'.

The same simulation has been repeated for all telescopes mentioned in Table 1, the resulting plots are shown in Appendix A.

For simulations five and six we change the cloud height to 5,000 km and 10,000 km respectively, the other parameters are kept the same as summarized in Table 2.

In Figure 7, in Appendix A, a zoom-in on the ingress of the light curve when  $h_{\text{cloud}} = 5,000$  km is shown. The effect of the cloud can clearly be discerned. The light curve of the cloudless planet falls outside of the  $1\sigma$ -interval (too small to be visible) around the cloudy planet mean light curve. In the plot of the residuals, not shown due to a lack of space, we see the pattern we were expecting to see, even in the noisy data (black dots). At ingress and egress a discrepancy of nearly 300 ppm occurs.

In Figure 8, in Appendix A, a zoom-in on the ingress of the light curve when  $h_{\text{cloud}} = 10,000$  km is shown. The effect of the cloud can clearly be discerned. The light curve of the cloudless planet falls outside of the  $3\sigma$ -interval (too small to be visible) around the cloudy planet mean light curve. In the plot of the residuals, not shown due to a lack of space, we see the pattern we were expecting to see, even in the noisy data (black dots). At ingress and egress a discrepancy of nearly 600 ppm occurs.

Our last simulation is based on the well parameterized exoplanet HD 260655 b. The only parameters that we weren't able to retrieve were the spin-orbit angle and the limb-darkening coefficients, so we chose them ourselves, assuming for limb-darkening a quadratic law. The resulting light curve and residual plot are shown in Figure 10 and Figure 11. A residual peak of about 150 ppm is reached.

Simulation	$R_*$ [ $R_\odot$ ]	$R_p$ [ $R_J$ ]	$h$ [km]	$a$ [AU]	$P$ [days]	$i$ [rad]	$\lambda$ [rad]	$u_n$ [–]	Tel. noise
1	1	1	2,100	0.1	11.5	$\frac{\pi}{2}$	0	0.69 <sup>a</sup>	NGTS
2	1	1	2,100	0.1	11.5	$\frac{\pi}{2}$	0	0.69 <sup>a</sup>	TESS
3	1	1	2,100	0.1	11.5	$\frac{\pi}{2}$	0	0.69 <sup>a</sup>	Kepler
4	1	1	2,100	0.1	11.5	$\frac{\pi}{2}$	0	0.69 <sup>a</sup>	CHEOPS
5	1	1	5,000	0.1	11.5	$\frac{\pi}{2}$	0	0.69 <sup>a</sup>	CHEOPS
6	1	1	10,000	0.1	11.5	$\frac{\pi}{2}$	0	0.69 <sup>a</sup>	CHEOPS
7 <sup>b</sup>	0.44	0.11	5,000	0.029	2.72	$\frac{87.35\pi}{180}$	$\frac{\pi}{4}$	[–0.19, 0.63]	CHEOPS

<sup>a</sup> taken from Moon et al. (2017).

<sup>b</sup> values of HD 260655 b taken from exoplanet.eu, except for the spin-orbit angle and the limb-darkening coefficients which are artificial.

Table 2: Overview of the parameters used during the simulations in order of appearance in the text/in appendix A.

## 4. Discussion

The effect of partial cloud coverage on a transiting planet's light curve can be seen in i.a. Figure 4. An asymmetry around phase = 0 arises. Depending on a trailing or a leading cloud coverage the light curve shifts to the right or left as compared to the cloudless planet, in the periodogram.

The effect is even better seen when plotting the residuals. In Figure 3 we see during ingress and egress a difference of about 100 ppm between the mean cloudy and cloudless planet light curves (red line). Because of the large noise in the data in Figure 3 we are not able to recognize this pattern in the actual, noisy data (black dots), however, in the residual plots for the CHEOPS and Kepler telescope

(unfortunately not shown due to a lack of space) it is possible. The uneven part in between the peaks in the residual plots are most likely due to a combination of limb-darkening and the inhomogeneous cloud coverage.

Looking at the light curves obtained for the four telescopes mentioned in Table 1 (Figures 2, 4, 5 and 6), we see that the large error on data obtained by NGTS and TESS makes it impossible to discern cloud coverage on the exoplanet simulated. When using the Kepler telescope and CHEOPS data, we should be able to recognize cloud coverage.

Looking at the light curves obtained for the three different cloud heights mentioned in Table 1, all simulated with CHEOPS' noise, (Figures 6, 7, 8), we see that there is a strong correlation between the cloud height and the asymmetry in the light curve. When we plot all of their individual residual lines in one graph (see Figure 9), we clearly see an increasing discrepancy with height between the cloudy and the cloudless planet, as expected.

Our seventh simulation tells us that if clouds of height  $\sim 5000$  km were present on HD 260655 b, both CHEOPS and Kepler should be able to observe them during ingress and egress.

The results of our (few) simulations correspond very well with other models mentioned in the literature such as the one by von Paris et al. (2016). The only major difference between their results and the ones mentioned in this paper are due to limb-darkening which they did not take into consideration.

## 5. Future prospects

Even though our model works exactly as desired, we believe there is still a lot that can be improved or added to obtain more realistic (or simply other existing) cases. Here we present a list of improvements or interesting additions for future work:

- **Spin-orbit angle**  $\lambda \rightarrow \frac{\pi}{2}$ . As mentioned before, to reduce the amount of computational time, we calculate the coordinates where the planet crosses the host star. The idea behind this approach is quite simple and works very well, except in the case where  $\lambda \rightarrow n \cdot \frac{\pi}{2}$  for  $n \in \mathbb{Z}$ , since the equation governing the planet's path contains  $\tan(\lambda)$  ( $\rightarrow \pm\infty$ ). For now, the exact case  $\lambda = \frac{\pi}{2}$  has been solved by explicitly adding a statement to find the intersections in a different manner. The problem with this approach is that if e.g.  $\lambda = \frac{\pi}{2} - \frac{\pi}{1,000,000}$  we still have a blown up  $\tan(\lambda)$  but the alternative calculation will not be used. We suggest a different way of handling such situations, which we weren't able to implement ourselves because of a lack of time. It might be better to define an interval of spin-orbit angles (e.g.  $n \cdot \frac{\pi}{2} \pm \frac{5\pi}{180}$  for  $n \in \mathbb{Z}$ ) for which the entire system (including the cloud) is rotated (counter)clockwise by  $\frac{\pi}{2}$  and the calculations proceed from this point on.
- **Eccentricity.** A fairly obvious extension of the model would be eccentricity. In the current state of the code, the assumption is made that  $e = 0$ . This is reasonable for a lot of planetary systems, still it might be interesting to include the more exotic cases as well.

- **Different shapes of cloud coverage.** Though research supports our current shape of cloud coverage (Lee et al. 2016), other shapes of cloud coverage have also been suggested (e.g. (Lines et al. 2018)). A code for predicting the effect of clouds on transit light curves is only complete with less strict conditions for the cloud coverage.
- **Time-variable cloud opacity.** Presently, our assumption is that the cloud is perfectly opaque and that this opaqueness is time invariant. As Helling (2019) mentioned the opacity of a cloud might vary in time as a consequence of temporary effects on the cloud's particle distribution. Mostly likely there will not be much change in opacity during the short time only the cloud is in transit, but a less opaque cloud might be a realistic scenario.
- **Oblateness.** Sphericity as an assumption is incorrect, neither host star nor transiting planet are perfect spheres in reality. Adjusting for this discrepancy and adding gravity darkening, as first predicted by von Zeipel, for the host star because of its oblateness can be done by incorporating the model by Barnes (2009). The influence this could have on the transit light curve is described in i.a. (Dholakia et al. 2022).
- **Stellar spots.** Adding stellar spots to the code shouldn't be too hard, the biggest disadvantage is the extra computational time and memory usage. Stellar spots, depending on their size, can have a major effect on the transit light curve and can easily be mistaken for exoplanets. Since the effect of a cloud on the light curve is seen during both the ingress and the egress, misinterpreting a stellar spot as a cloud is highly unlikely (because it would need to appear and disappear at exactly the same time as planetary ingress and egress).
- **Multiple planets.** In future versions multiple planets might be added. Our own solar system contains multiple planets and other stellar systems have also been shown to have more than one planet. Like for stellar spots, the downside of adding more planets is the amount of memory storage and computational time necessary.
- **Inverse model.** Once the model includes every factor we want it to include, we should reverse the procedure. We should look at the derived light curves and try to retrieve the original parameters. For this the Bayesian formalism to calculate posterior probability values for the parameters given an amount of observations should be used, as is done by (von Paris et al. 2016).

## 6. Conclusion

We have presented our model for the simulation of the effect of partial cloud coverage on light curves of exoplanet. The cloud will cause an asymmetry in the light curve.

We have shown that depending on both the bulk and orbital parameters of the exoplanet and the telescope used for observation, the discrepancy should (not) be observable.

Eventhough we have demonstrated that the code works correctly, we recognize the fact that there is still room for improvement. We have made some suggestions ourselves for future improvements.

*Acknowledgements.* I would like to express my gratitude to my supervisor, Sven Kiefer, who guided me throughout this interesting project. Whenever I had any questions or doubts, I could turn to him.

## References

- Barnes, J. W. 2009, *The Astrophysical Journal*, 705, 683
- Benz, W., Broeg, C., Fortier, A., et al. 2021, *Experimental Astronomy*, 51, 1
- Campante, T. L., Schofield, M., Kuszlewicz, J. S., et al. 2016, *The Astrophysical Journal*, 830, 138
- Charbonneau, D., Brown, T. M., Noyes, R. W., & Gilliland, R. L. 2002, *The Astrophysical Journal*, 568, 377
- Dholakia, S., Luger, R., & Dholakia, S. 2022, *The Astrophysical Journal*, 925, 185
- Esteves, L. J., Mooij, E. J. W. D., & Jayawardhana, R. 2015, *The Astrophysical Journal*, 804, 150
- Gilliland, R. L., Chaplin, W. J., Dunham, E. W., et al. 2011, *The Astrophysical Journal Supplement Series*, 197, 6
- Giménez, A. 2006, *AA*, 450, 1231
- Gizon, L., Sekii, T., Takata, M., et al. 2016, *Science Advances*, 2, e1601777, doi: 10.1126/sciadv.1601777
- Helling, C. 2019, *Annual Review of Earth and Planetary Sciences*, 47, 583, doi: 10.1146/annurev-earth-053018-060401
- Lee, E., Dobbs-Dixon, I., Helling, C., Bognar, K., & Woitke, P. 2016, *AA*, 594
- Lines, S., Mayne, N. J., Boutle, I. A., et al. 2018, *AA*, 615
- Mandel, K. & Agol, E. 2002, *The Astrophysical Journal*, 580, L171
- Moon, B., Jeong, D.-G., Oh, S., & Sohn, J. 2017, *Journal of Astronomy and Space Sciences*, 34, 99
- von Paris, P., Gratier, P., Bordé, P., Leconte, J., & Selsis, F. 2016, *AA*, 589
- Wheatley, P., West, R., Goad, M., et al. 2017, *Monthly Notices of the Royal Astronomical Society*, 475
- Wolszczan, A. & Frail, D. A. 1992, *Nature*, 355, 145

## A. More plots

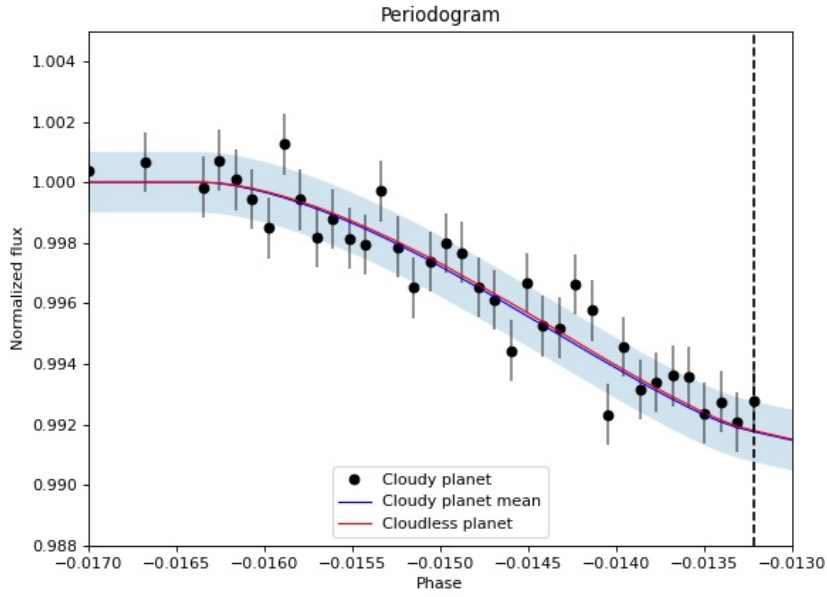


Figure 4: Zoom-in on the light curve obtained for a Jupiter-like planet with  $h_{\text{cloud}} = 2, 100$  km passing in front of a sun-like star. The noise resembles TESS', the light blue region is the  $1\sigma$ -interval around the cloudy planet's mean light curve. The black dotted line shows the end of ingress.

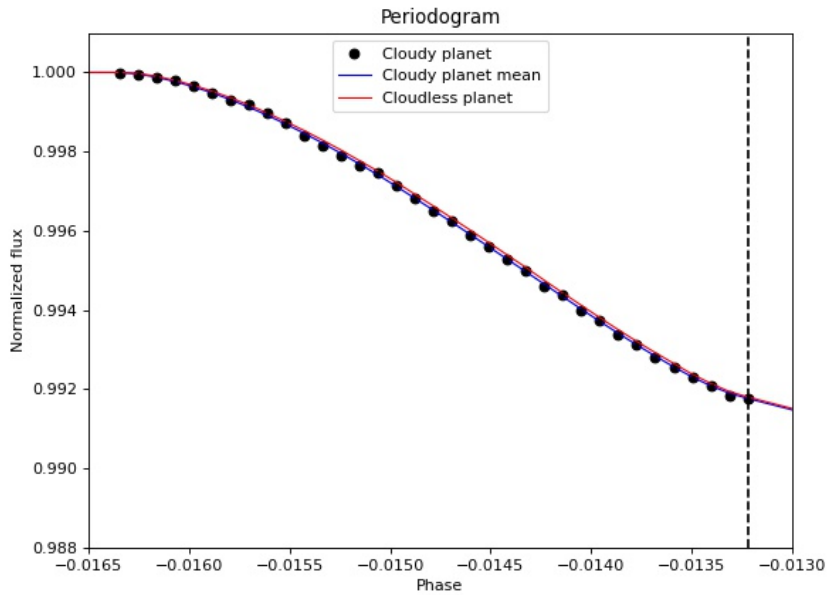


Figure 5: Zoom-in on the light curve obtained for a Jupiter-like planet with  $h_{\text{cloud}} = 2, 100$  km passing in front of a sun-like star. The cloudy planet's mean light curve, in blue, seems a bit shifted to the left. The noise resembles Kepler's, error bars and  $3\sigma$ -interval (in light blue) are hard to see because of Kepler's high precision. The black dotted line shows the end of ingress.

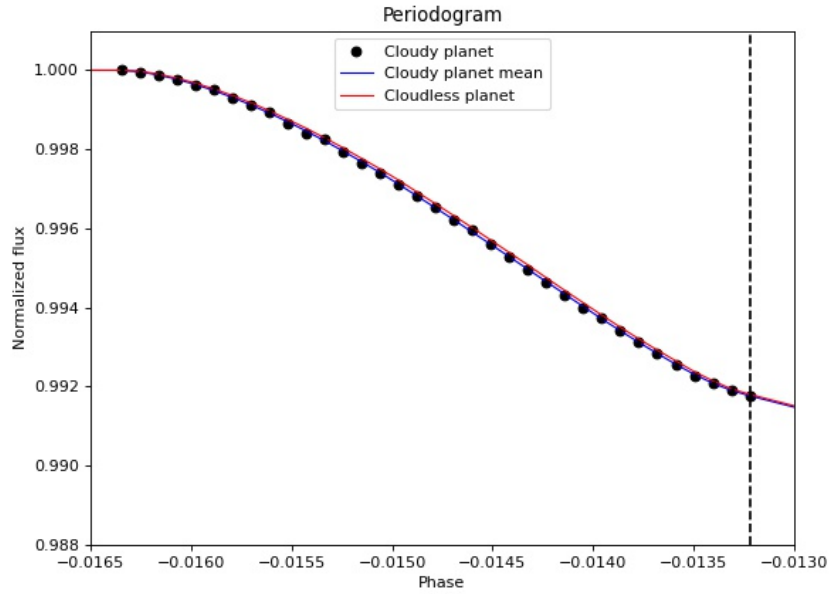


Figure 6: Zoom-in on the light curve obtained for a Jupiter-like planet with  $h_{\text{cloud}} = 2, 100$  km passing in front of a sun-like star. The cloudy planet's mean light curve, in blue, seems a bit shifted to the left. The noise resembles CHEOPS', error bars and  $3\sigma$ -interval (in light blue) are too small to see because of CHEOPS' high precision. The black dotted line shows the end of ingress.

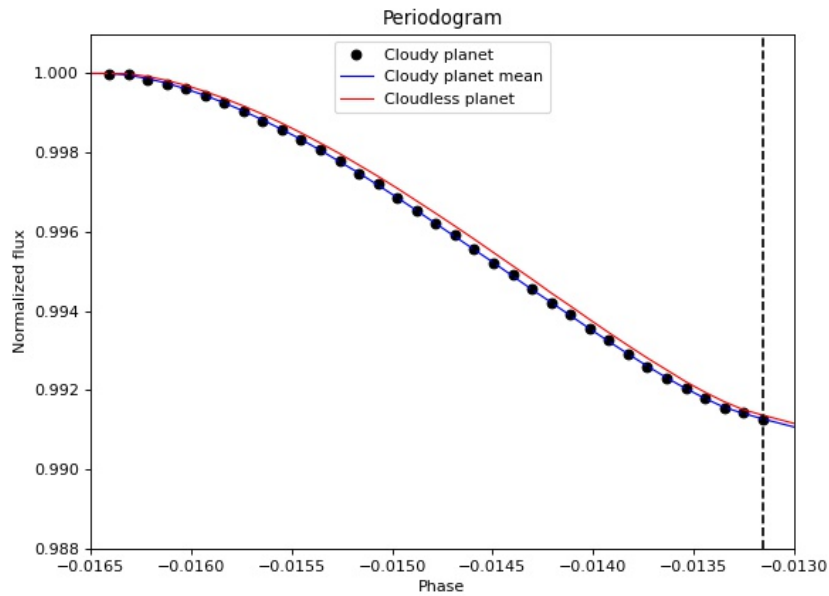


Figure 7: Zoom-in on the light curve obtained for a Jupiter-like planet with  $h_{\text{cloud}} = 5, 000$  km passing in front of a sun-like star. The cloudy planet's mean light curve, in blue, seems a bit shifted to the left. The noise resembles CHEOPS', error bars and  $1\sigma$ -interval (in light blue) are too small to see because of CHEOPS' high precision. The black dotted line shows the end of ingress.

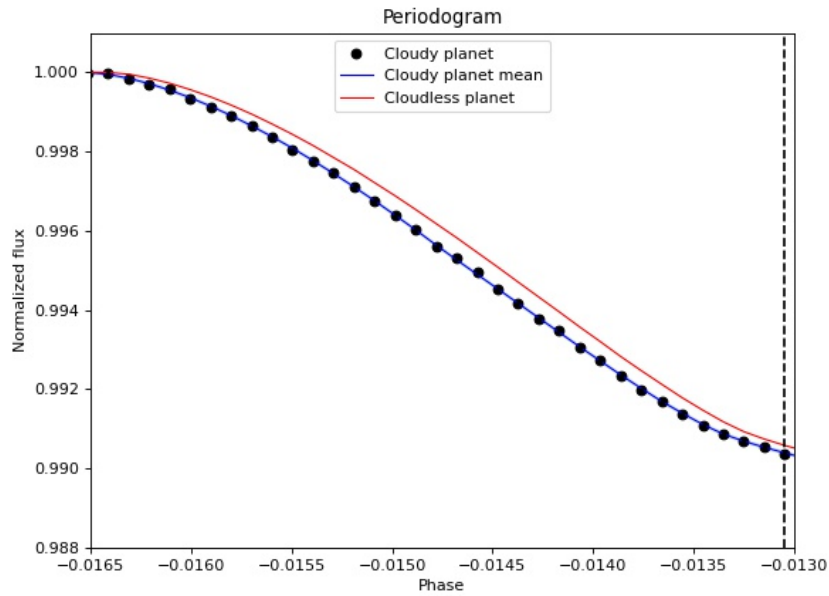


Figure 8: Zoom-in on the light curve obtained for a Jupiter-like planet with  $h_{\text{cloud}} = 10,000$  km passing in front of a sun-like star. The cloudy planet's mean light curve, in blue, seems a bit shifted to the left. The noise resembles CHEOPS', error bars and  $3\sigma$ -interval (in light blue) are too small to see because of CHEOPS' high precision. The black dotted line shows the end of ingress.

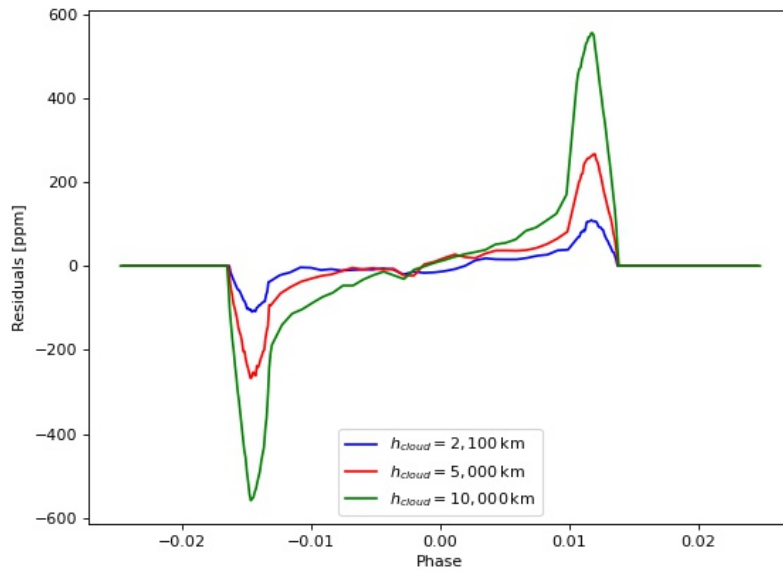


Figure 9: A plot with the residual lines for a Jupiter-like planet with varying cloud height passing in front of a sun-like star. A clear correlation between cloud height and discrepancy can be seen.

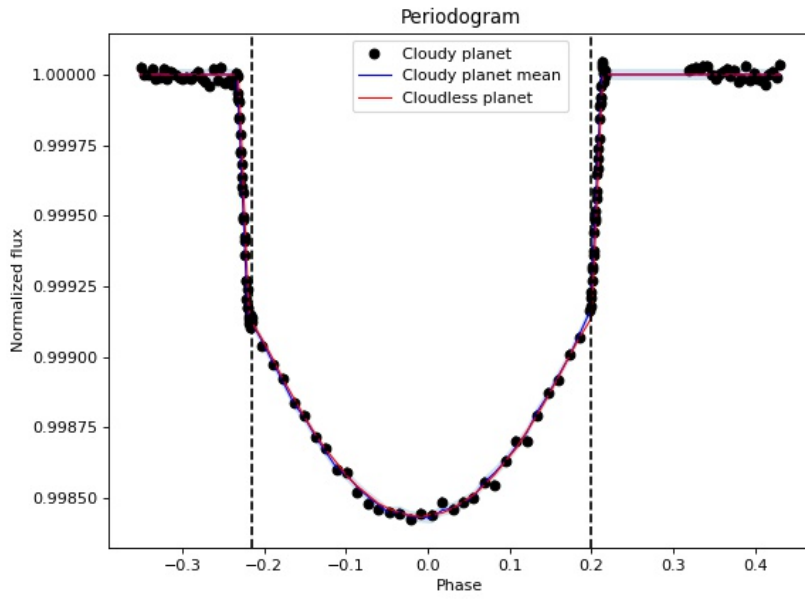


Figure 10: The light curve obtained for HD 260655 b with  $h_{\text{cloud}} = 5,000$  km. The noise resembles CHEOPS', error bars and  $1\sigma$ -interval (in light blue) are barely visible because of CHEOPS' high precision. The black dotted line shows the end of ingress.

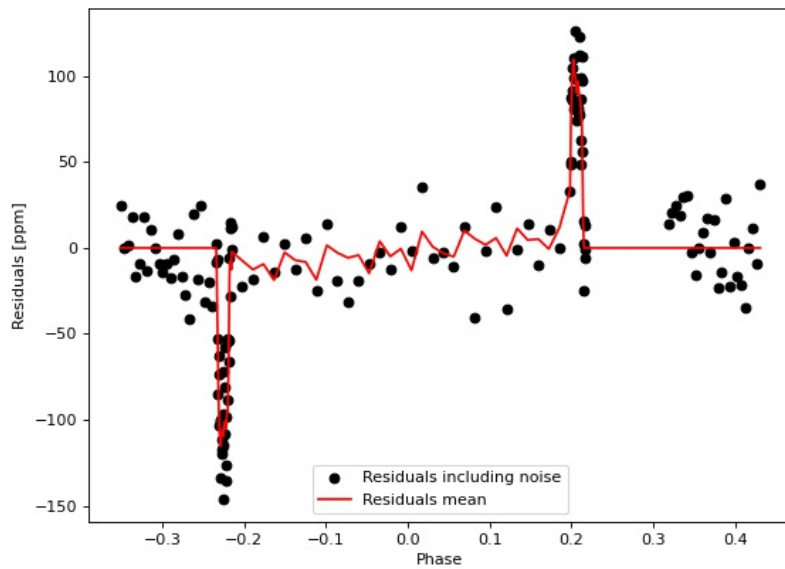


Figure 11: The residuals between a symmetric and an asymmetric model obtained for HD 260655 b with  $h_{\text{cloud}} = 5,000$  km. The noise resembles CHEOPS'.